Pergamon

Acta mater. 49 (2001) 3443–3451

Acta MATERIALIA

www.elsevier.com/locate/actamat

GP-ZONES IN Al–Zn–Mg ALLOYS AND THEIR ROLE IN ARTIFICIAL AGING

L. K. BERG[1], J. GJØNNES[1]†, V. HANSEN‡[1], X. Z. LI§[1], M. KNUTSON-WEDEL[2], G. WATERLOO[3], D. SCHRYVERS[4] and L. R. WALLENBERG[5]

[1]Center for Materials Science, University of Oslo, Gaustadalleen 21, N-0349, Oslo, Norway, [2]Chalmers Technical University, S-41296, Göteborg, Sweden, [3]Hydro Automotive Structures, Raufoss, PO Box 15, N-2831 Raufoss, Norway, [4]University of Antwerp, RUCA, EMAT, Groenenborgerlaan 171, Antwerp, B-2020, Belgium and [5]Inorganic Chemistry 2, Chemical Center, Lund University, Box 124, S-22100 Lund, Sweden

(Received 14 February 2001; received in revised form 15 June 2001; accepted 15 June 2001)

Abstract—The structure of GP-zones in an industrial, 7xxx-series Al–Zn–Mg alloy has been investigated by transmission electron microscopy methods: selected area diffraction, conventional and high-resolution imaging. Two types of GP-zones, GP(I) and (II) are characterized by their electron diffraction patterns. GP(I)-zones are formed over a wide temperature range, from room temperature to 140–150°C, independently of quenching temperature. The GP(I)-zones are coherent with the aluminum matrix, with internal ordering of Zn and Al/Mg on the matrix lattice, suggested to be based on AuCu(I)-type sub-unit, and anti-phase boundaries. GP(II) are formed after quenching from temperatures above 450°C, by aging at temperatures above 70°C. The GP(II)-zones are described as zinc-rich layers on {111}-planes, with internal order in the form of elongated <110> domains. The structural relation to the η'-precipitate is discussed. © *2001 Acta Materialia Inc. Published by Elsevier Science Ltd. All rights reserved.*

Keywords: Aluminum alloys; Transmission electron microscopy (TEM); Electron diffraction; Nucleation, growth; Guinier–Preston zones

1. INTRODUCTION

Guinier–Preston, or GP-zones have been recognized as microstructural elements in aluminum alloys since the early work of Guinier [1] and Preston [2]. The zones are formed by "natural aging" at room temperature, and in early stages of the industrially important "artificial aging" at temperatures in a range 100–180°C. However, their precise role in the formation of hardening precipitates is still not clear in most alloys. Transformation schemes quoted in textbooks or review articles, e.g.

$$\text{solid solution}(\alpha)\rightarrow\text{GP-zones}\rightarrow\eta'\rightarrow\eta\text{-MgZn}_2 \quad (1)$$

for artificial aging in the Al–Zn–Mg precipitation hardening 7xxx-alloys, are simplifications. The equilibrium phase, η, is a hexagonal Laves phase, with $a = 0.5221$ nm, $c = 0.8567$ nm [3, 4]. A large number of orientation relations to the aluminum matrix have been reported [5, 6]. The main hardening precipitate η', is a metastable hexagonal phase, semi-coherent with the aluminum matrix ($a = 0.496$ nm$\cong[211]/2_{Al}$; $c = 1.40$ nm$\cong 2[111]_{Al}$, where $a_{Al} = 0.405$ nm). Structure models for η' have been proposed from X-ray diffraction [7], and recently from HRTEM [8]. Structural relations between the aluminum matrix, η' and η-$MgZn_2$ were discussed in [8, 9]. Evidence for internal order in GP-zones in the system, and for the existence of several types of zones was first presented by Schmalzried and Gerold [10].

Early experimental studies of precipitate hardening were interpreted in different ways. Graf [11] observed GP-zones only at low-temperatures, and assumed that a metastable hardening precipitate phase η', is formed directly from the solid solution at temperatures above 100–120°C. On the other hand, Lorimer and Nicholson [12] proposed that GP-zones serve as nuclei for η' in a two-stage aging process, whereas Pashley *et al.* [13] suggested that η' is formed from stable clusters. Later Lyman and VanderSande [14] observed

† To whom correspondence should be addressed.
E-mail address: jon.gjonnes@fys.uio.no (J. Gjønnes)
‡ Present address: Stavanger University College, Department of Technology and Natural Sciences, P.O. Box 2557, Ullandhaug N-4091 Stavanger, Norway
§ Present address: Center for Materials Research and Analysis, 112 Brace Laboratory, P.O. Box 880113, Lincoln, NE 68588-0113, USA

1359-6454/01/$20.00
PII: S1359-6454(01)00251-8

hexagonal, coherent particles in transmission electron micrographs at early stages of aging at 150°C, as possible precursors to η'.

In industrial praxis precipitation hardening is preceded by rapid quenching from a sufficiently high solution temperature, around 500°C, before a two-stage aging treatment, e.g. at 100°C and 150°C. Several investigators, [15–19], concluded that vacancies retained during the quench must have a significant role in the precipitation process. However, it seemed that the quenched-in vacancies have little influence on room temperature aging, and hence on the formation of GP-zones in the low-temperature region, below 80–100°C. These observations were discussed in detail by Katz and Ryum [18], in terms of vacancy-rich clusters (VRC). It followed that the clusters must be formed during or immediately after quenching, and be stable enough to be active at subsequent aging at 150°C. Hence the precipitation sequence

$$\text{solid solution}(\alpha) \rightarrow \text{VRC} \rightarrow \eta' \rightarrow \eta\text{-MgZn}_2 \qquad (2)$$

for aging at 150°C, when the specimen had first been quenched to room temperature before the aging treatment. In addition the equilibrium phase η can be formed directly from the solid solution. The sequence (1) may also occur, notably after direct quenching to the aging temperature. This description explained the hardening response to aging over a wide range of temperature conditions and solution pre-treatment. However, the role and structure of zones and clusters during the early stage of aging remained unclear. The evidence for the existence of VRC were indirect, cf. the remark in a recent review article [20]: "no direct observation has ever been reported, e.g. on the size, structure or composition of the VRC".

Formation and growth of GP-zones in aluminum alloys can be followed by several kinds of measurements. Indirectly by mechanical measurements, such as hardness and flow stress; electrical conductivity; calorimetry (DSC) [21, 22]; positron annihilation [23, 24] magnetic susceptibility [25]. Structure information has been obtained by diffraction methods using either X-rays (including small-angle scattering, SAXS) or electrons, and by electron microscope imaging. In their early X-ray studies of the Al–Zn–Mg system Schmalzried and Gerold [10] found strong diffuse scattering around the matrix positions 100, 201, 003 etc. in natural aged alloys, and concluded that the zones must be ordered. As a model they suggested alternating {100} planes of Zn and Mg, as in CuAu(I)-type ordering, and indicated that another kind of zones may be formed at somewhat higher temperatures. Subsequent studies by small-angle scattering, e.g. [26], were aimed at estimating the zinc content, by utilizing the difference between the scattering amplitude of zinc and that of aluminum or magnesium. Early electron microscopy studies in conventional bright-field and dark field modes, and diffraction [5, 6, 27] were concerned mainly with the precipitate phases. TEM images revealing GP-zones distributions were reported [16, 28]; less attention seems to have been paid to their internal structure. Later investigations confirmed the existence of a high-temperature type [14, 29] as "spherical hexagonal zones" or as thin platelets on {111} [30, 31]. The first HRTEM images of GP-zones published for this system are due to Mukhopadhyay [32], who showed contrast effects attributed to spherical zones with diameter 3–5 nm, from samples aged at room temperature and 95°C. The contrast was either enhanced or reduced relative to the surrounding matrix; this was interpreted to be due to zones enriched in either Zn or Mg, with no indication of internal order. The composition of the zones has been studied with atom probe (APFIM). Ortner [30] reported an approximate composition Al_6ZnMg, while Hono *et al*. [33] found 20–25at% Zn, 10–15% Mg, 2% Cu. Stiller *et al*. [34] found a large spread in the Zn/Mg ratio around a mean value of 1.2 for zones formed at 100°C.

We have undertaken structure studies with TEM of the metastable precipitates and zones that occur during artificial two-stage aging in the Al–Zn–Mg alloy system. A new structure model for the metastable phase η' has already been published [8]. In the present article some results from electron diffraction and high resolution microscopy of GP-zones in commercial Al–Zn–Mg alloys in the 7xxx-series alloys are reported. A survey of diffraction features observed at the early stages in the aging treatment is presented, and interpreted in terms of two types of GP-zones, I and II. A model for the internal order in GP(I)-zones is proposed. Possible models for GP(II), and the relation to η' and η-$MgZn_2$ are discussed on the basis of HRTEM and electron diffraction evidence.

2. EXPERIMENTAL

Several industrial Al–Zn–Mg alloys were included in our investigations; the results reported here refer to an AA7108-alloy with main alloying elements 5.36% Zn, 1.21% Mg and 0.16% Zr (wt%). Zr is added in order to produce cubic Al_3Zr dispersoids, which produce sharp extra spots at the positions 100_{Al}, etc. in the diffraction patterns. Prior to the aging treatment the industrial alloys had been extruded and solution treated at 480°C. Artificial aging was performed according to industrial practice, in two stages: 5 h at 100°C, followed by further aging at 150°C. Specimens for electron microscopy (TEM) investigations were prepared from material at different stages during the double aging treatment, which extended to so-called T6 (optimal hardness) and T7-states (over-aged). Some samples were also studied after natural (room temperature) aging. A major part of the results presented here refer to the 100°C intermediate stage. Another set of aging experiments were

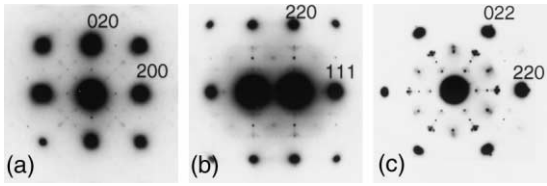

Fig. 1. Selected area diffraction patterns (SAED) from samples aged to T6 state: 5 h at 100°C +6 h at 150°C. (a) $[001]_{Al}$-projection; (b) $[112]_{Al}$-projection, (c) $[111]_{Al}$-projection. Precipitate spots are from η′. Sharp extra spots at simple cubic positions 100_{Al} etc. are from the Al_3Zr dispersoids.

performed at temperatures ranging from 70 to 140°C, results from these will be reported elsewhere. The TEM investigations included selected area electron diffraction, conventional (CTEM) bright-field and dark field microscopy as well as high resolution microscopy (HRTEM). The following instruments have been used: JEOL 200CX, 2000FX, 4000EX, and LEO 912. The last one is equipped with an energy filter, which has considerable advantages for recording weak and diffuse spots from precipitates in an alloy matrix, and was used for the majority of the reproduced diffraction patterns. TEM thin foils were prepared by electropolishing in a mixture of 70% methanol, 20% glycerol and 10% perchloric acid, cooled to −20°C with liquid nitrogen. Some measurements of hardness, electrical conductivity and yield stress during room temperature aging are reported in [35].

3. RESULTS

3.1. Electron diffraction

Electron diffraction patterns were taken in the selected area (SAED) mode, after aging at different temperatures, and at several stages during the industrial double aging procedure. The main aluminum projections used are <001>, <111> and <112>; special attention was directed to diffuse scattering features. Patterns from samples aged to the T6-state, Fig. 1, (with reflections from the metastable hardening phase η'), and from the over-aged T7-state, Fig. 2, (with η-$MgZn_2$ as the main precipitate) are shown for comparison. In patterns taken from samples aged at 100°C for 1.5–5 h, Fig. 3(a–c), two characteristic patterns of diffuse spots were identified, and associated with the GP-zones GP(I) and GP(II) respectively. Diffraction patterns from GP(I) are best viewed in the $[001]_{Al}$ projections, Fig. 3(a). Rows of diffuse spots can be indexed as $hkl = 1,(2n + 1)/4,0$ in the aluminum reciprocal lattice, corresponding to a tetragonal or orthorhombic anti-phase structure, with a four-doubling along one cubic axis. The strongest diffuse spots from GP(I) appeared at positions $1,1/4,0_{Al}$ and $1,7/4,0_{Al}$. Similar, but weaker patterns were observed also after room-temperature (natural) aging.

Patterns associated with GP(II)-zones are shown in Fig. 3(b), $[112]_{Al}$, and Fig. 3(c) $[111]_{Al}$ projections. In Fig. 3(c) strong diffuse spots appear slightly outside $\{422\}/3_{Al}$ positions. The spots are frequently of complicated shape. In Fig. 4(a), sets of three spots are seen around the $\{422\}/3_{Al}$ positions, elongated in three different <110> directions; the spots on the radial $<422>_{Al}$ direction being the strongest. The other two spots in the group could be the result of double scattering via a 220-type matrix reflection. The *d*-value 0.23 nm, corresponding to the strong radial spot, is 6–8% less than $d_{422}/3_{Al}$ On tilting the specimen, as shown by Fig. 4(b and c), we found the diffuse spots to be intersections with strong $<111>_{Al}$ diffuse streaks that extend between e.g. 111_{Al} and 200_{Al} The streaks can be seen also in $<110>_{Al}$ projections, Fig. 5(c), but here with much weaker contrast. It may be mentioned here that also spots from the precipitate phase η' appear weaker when recorded in $<110>_{Al}$. A third feature of diffuse scattering is seen in Fig. 5 (a and b), as arcs slightly inside the 200 matrix reflection. The arcs are visible in several projections, most notable after short aging times, as in Fig. 5(a).

The GP(I) and GP(II)-zones are formed in different temperature ranges. GP(I) was found after aging at room temperature, and up to about 140°C. GP(II)-zones are formed mainly above 70°C; at lower temperatures they have been observed only occasionally in samples that had been aged for very long time (several weeks or more). Type II patterns were not found after quenching from temperatures at or below 450°C. This indicates that the GP(II)-zones depend on a high supersaturation of quenched-in vacancies,

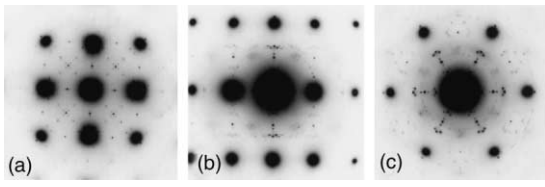

Fig. 2. SAED patterns from T7 state, the 150°C aging extended to 24 h. (a) [001]; (b) [112]; (c) [111] projection. Most precipitate spots are here from η-$MgZn_2$ in the orientations η_1 and η_2 [6].

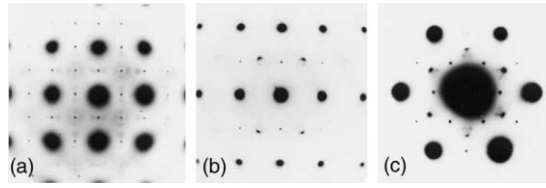

Fig. 3. SAED patterns along [010] from samples aged for 1.5 h at 100°C. (a) [001]-projection, with GP(I)-type diffuse spots at positions {1,1/4,0} etc.; (b) [112] projection with diffuse GP(II)-spots near {311}/2, and c: [111]-projection (unfiltered), with GP(II)-spots near {422}/3 positions. (Indices refer to Al matrix).

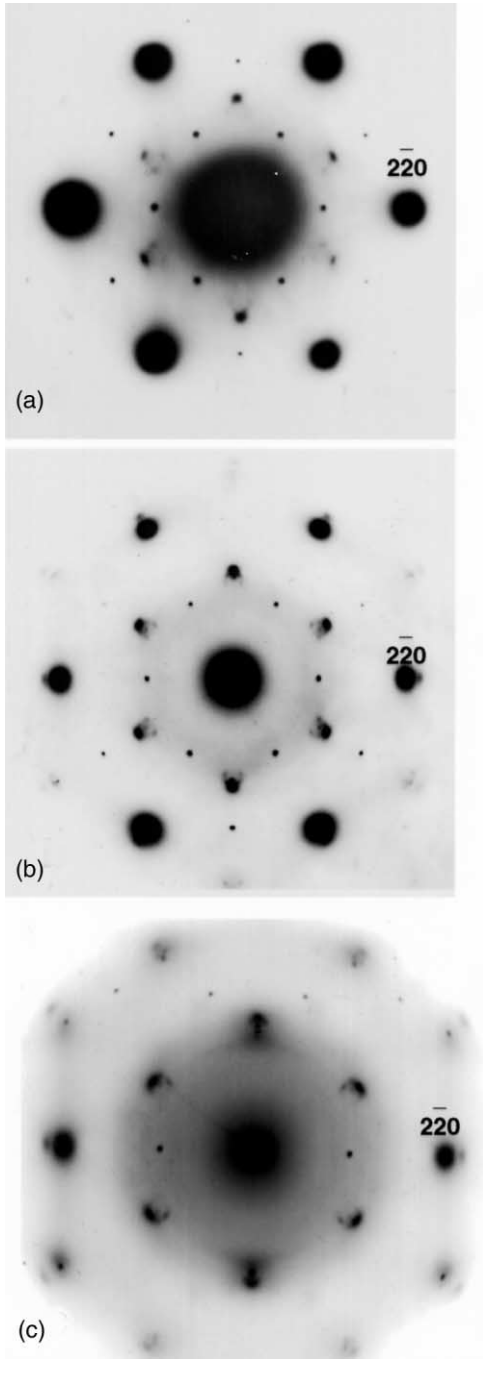

Fig. 4. Examples of SAED-patterns with diffuse spots from GP(II), near [111]-projection. Sample aged for 3 h at 100°C. (a) (unfiltered): distinct three-fold split of spots around {224}/3-type spots. (b) and (c) are from the same grain; (c) tilted off [111] towards [332]-projection, the diffuse spots remain.

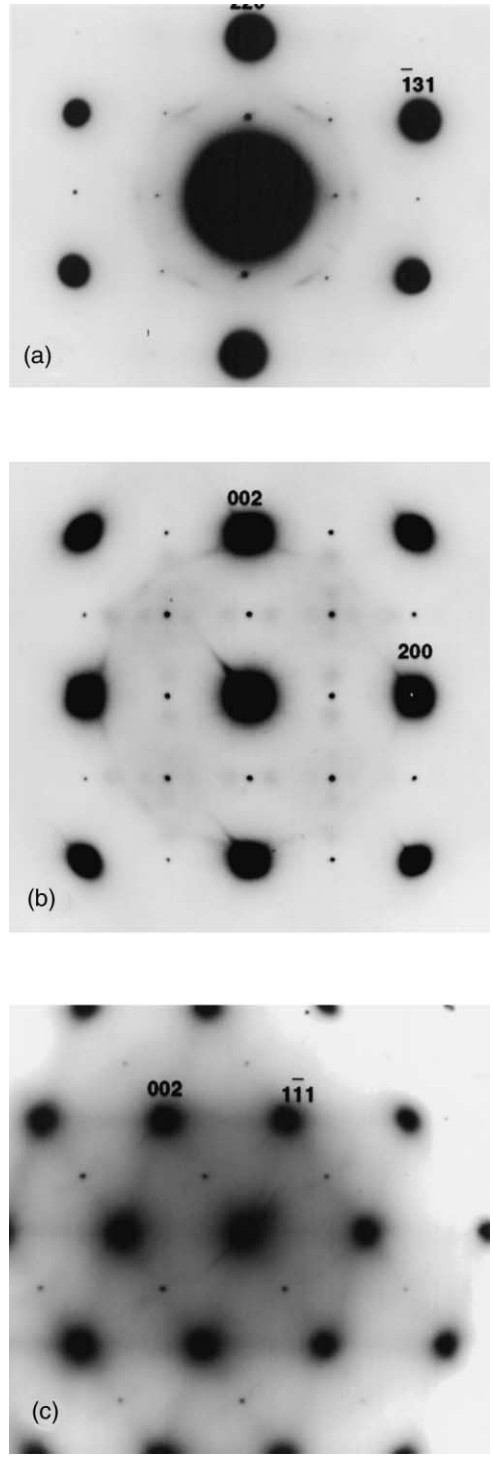

Fig. 5. SAED patterns with diffuse arcs and streaks. Samples aged at 100°C (a) (unfiltered): aged 0.5 h, [411]-projection; (b) aged 1.5 h, [001]-projection; (c) aged 1.5 h, [011]-projection with weak <111> diffuse streaks.

as has been assumed for the "vacancy-rich clusters" [17]. Considerable variations in the intensity of type II-patterns occurred, even between grains in the same sample. Differences in intensities between the three sets of GP(II)-spots in a <111>-projection were sometimes noted.

3.2. Conventional electron microscopy. Bright-field and dark-field images

GP(I) zones were imaged readily in $<100>_{Al}$ projections. In bright-field images, Fig. 6, the zones

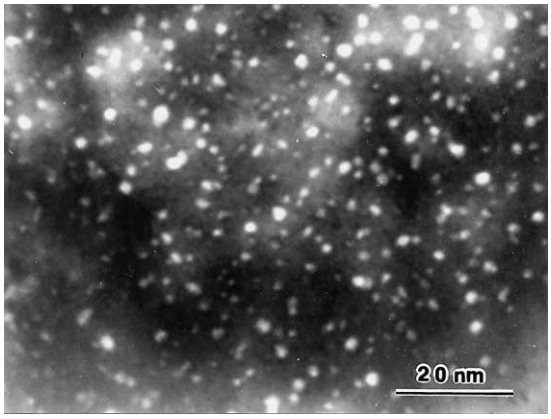

Fig. 6. Bright-field image of GP(I)-zones, [001]-projection.

appear with bright or dark contrast, depending on diffraction condition. Typical zone size after 1.5 h aging at 100°C were 1.5–3 nm, increasing only slowly with further aging. At higher aging temperatures, the zones are somewhat larger, 2–3 nm. The GP(II)-zones are more difficult to image by diffraction contrast. A typical dark-field image taken in [111]-projection from the strong diffuse spots at a 422/3-type position is shown as Fig. 7. The contrast is irregular; individual particles are difficult to discern.

3.3. High-resolution electron microscopy

High resolution images were taken in the Al-projections <100>, <110>, <111> and <211>. Images obtained from T6-specimens in the last two projections revealed η'-particles, as described by Li *et al.* [8]. Specimens aged at 100°C for 1.5 h were selected for imaging GP-zones. Contrast features in the [110] projection, Fig. 8(a and b), were identified as GP(II)-zones, which appear as thin objects parallel to {111}-planes, 1–2 atom layers thick, 3–6 nm wide. In <112>-projections no faults of this type could be discerned. However, some larger particles about 10 nm wide and approximately 10 atom layers thick

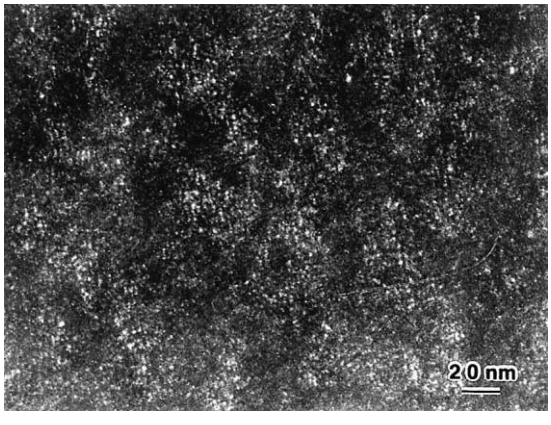

Fig. 7. Dark-field image of GP(II)-zones taken with a diffuse (422)/3-spot near [111] projection, showing weak, irregular contrast.

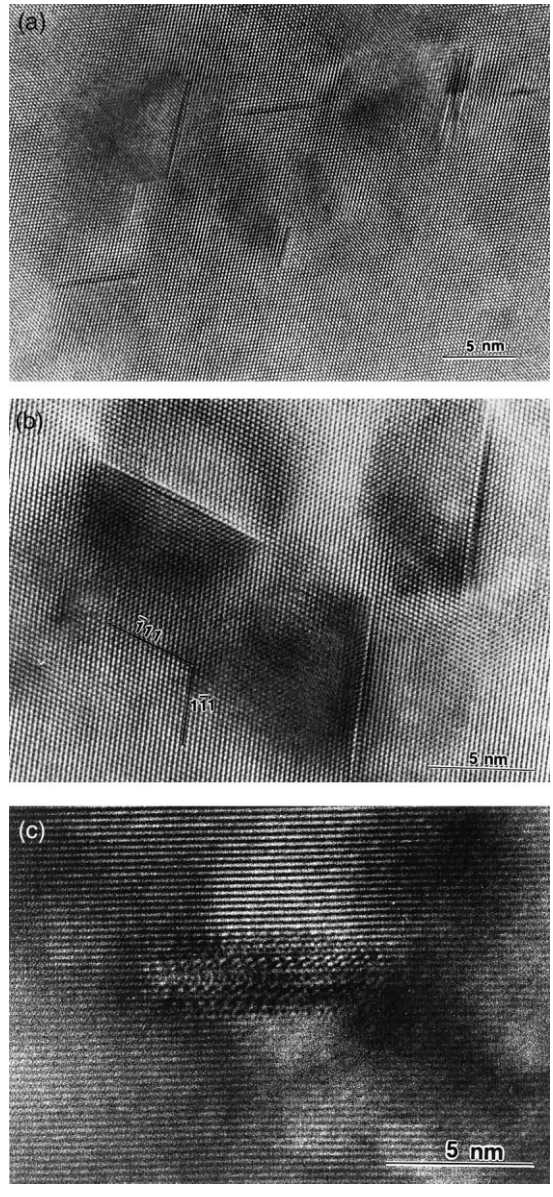

Fig. 8. HRTEM images in [110] projection, showing GP(II)-zones as {111}-layers on or two atoms thick in two magnifications, (a) and (b), note strain field on one side of zone; (c) thicker zone or precipitate on (111)-plane, a possible transition stage in the formation of η'.

were found, Fig. 8(c), with some resemblance to particles seen in micrographs from the T6-state [8]. These were assumed to be an early stage in the formation of η'-precipitates. In order to obtain further information about the structure of GP(II)-zones, high-resolution images were recorded also in $<111>_{Al}$ projections, with an aperture chosen to reduce contribution from {220} matrix reflections. The contrast from zones was very weak; only by careful inspection of prints and negatives could fringes be seen in parts of several small areas, a few nm wide, Fig. 9. Measurement of fringe distances gave 0.23 nm, in good agreement with the *d*-value deduced from the

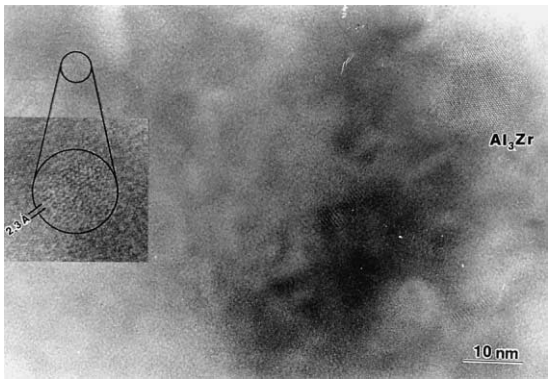

Fig. 9. HRTEM image of GP(II)-zones in [111]-projection (a) with inset (b), showing the 0.23 nm spacing.

GP(II)-spots in $<111>_{Al}$ diffraction patterns. HRTEM micrographs in $<001>_{Al}$ projections were taken in an attempt to reveal GP(I); only some faint contrast features were found. Some round areas with contrast level different from the surrounding area were seen, and may resemble those reported by Mukhopadhyay [32].

4. DISCUSSION

Two types of GP-zones, GP(I) and GP(II), and their domains of appearance, have been characterized by their electron diffraction patterns. The two types are best observed in the $<100>_{Al}$ and $<111>_{Al}$ projections respectively. The GP(I) patterns indicate fully coherent zones, with internal order described by a four-doubling of the aluminum cell in one cube direction. This can be compared with the atomic order suggested by Schmalzried and Gerold [10], viz. an AuCu (I)-type arrangement of alternate magnesium and zinc planes. Their argument was based on strong diffuse scattering around 100 positions in the reciprocal lattice of the matrix, compared to the 110-type positions. More details are seen in the electron diffraction patterns; diffuse spots appear at $1,(2n + 1)/4,0_{Al}$, and can thus be indexed as $1l0$, with $l = 2n + 1$, in a tetragonal or orthorhombic supercell. This suggests a periodic anti-phase structure built from the AuCu(I)-type basic unit [10], see Fig. 10. Note that the $[001]_{Al}$ projection shown will reproduce the observed intensity differences along the $1l0$ row of diffuse spots. The intensity ratios for the $0l1$ row will be different in the other, $[100]_{Al}$ projection. However, faults and size effects resulting from the differences in atomic radii between Mg, Al and Zn may influence the intensities; a more detailed model does not seem possible at this stage. Attempts to observe these ordered zones by HRTEM images in $[100]_{Al}$ projection failed, possibly because the order is incomplete, as is indicated by the width of the diffuse spots. The GP(I) zones are formed over a wide range of aging temperatures (including room temperature), and quenching temperatures. This is in contrast to GP(II), which were found only after quenching from temperatures above 450°C. Atom probe observations [34] indicate that both Zn and Mg are present in GP(I) zones, which may be spherical [32].

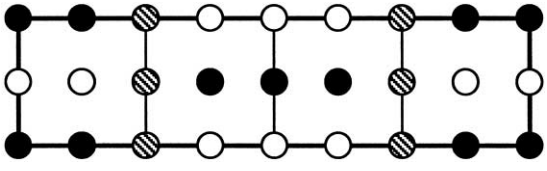

Fig. 10. Projected antiphase structure similar to CuAu (II) along [001], consistent with the diffuse spots from GP(I)-zone, cf. Fig. 3(a). Zn atoms as filled circles, Mg (or Al) as open circles; hatched circles indicate disorder at these sites.

The GP(II)-zones could be imaged quite readily by HRTEM in $<110>_{Al}$ projections. The zones appear as thin layers on {111}-planes edge-on, one-to-two atoms thick, and 3–5 nm wide. Dark or bright contrast on one side of the layers indicate an associated strain-field. The diffuse diffraction spots seen just outside the $422/3_{Al}$ positions in $<111>$ projections are consistent with single {111} layer of atoms with scattering power different from the matrix. These atoms will most likely be zinc, as has been found by X-ray analysis (XEDS) in TEM [30]. More details are suggested by the triangular fine structure of the group of three diffraction spots near each {422}/3, see Fig. 11(a): a tangential $<110>$-streak through the main spots outside {422}/3, and streaks in the other $<110>$-directions through the weaker satellites. The streaking of the spots in three directions can be explained by three different orientations of GP(II)-zones on one set of $\{111\}_{Al}$-planes. Or by three domain orientations within the zones, which appears more likely, and is consistent with HRTEM images along $<111>_{Al}$. The satellites may be the result of double diffraction via matrix reflections.

Diffraction patterns and HREM images can then be interpreted in this way: GP(II)-zones are planar {111} sheets with high content of zinc. Within the sheets the local order is associated with three sets of domains elongated in $<110>$-directions, and with a spacing between rows of atoms some 6–8% less than in the aluminum matrix. We assume that this reduced spacing, relative to the aluminum layers above or below the sheet, is associated with the smaller radius of Zn-atoms. This contraction must be accommodated to the surrounding matrix in a coherent fashion, since there is no indication of misfit. Two mechanisms may be invoked: (i) the contraction can occur in domains along three directions, which will reduce the average reduction of spacing by about a half, or (ii) magnesium atoms, with radius nearly 12% larger than aluminum, can produce local lattice expansion and relieve part of the strain from the contraction due to zinc. The latter mechanism is similar to the model previously suggested for the transition between the aluminum matrix and the η'-precipitate [8]; see Fig. 12, where displacements of the atoms in the planar Zn-layer

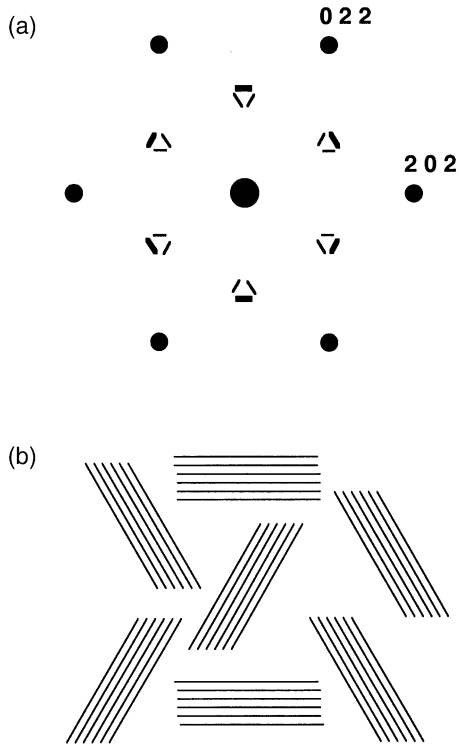

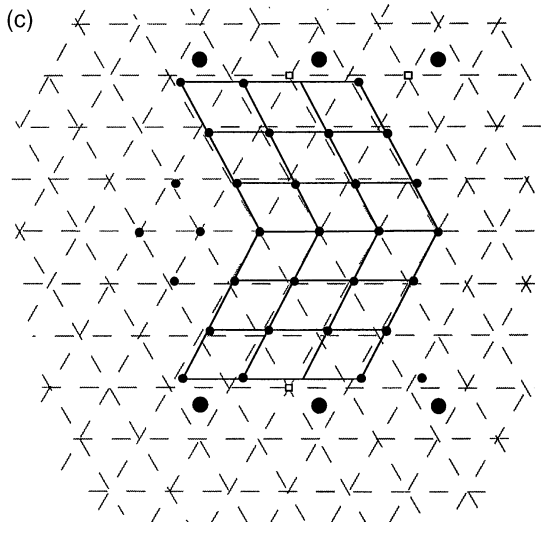

Fig. 11. Elements in a possible GP(II)-model. (a) sketch of observed diffuse spots around {224}/3 positions, cf. Fig. 4(a), large circular spots are matrix reflexions; (b) suggestive mosaic domain structure within one GP(II)-zone: Zn-rich rows along three <110>-directions; (c) large Mg-atoms (large filled circles) in neighbouring layer may relieve the <211>-contraction between the zinc-rows. The triangular net (three <110>-directions) indicate one (111) layer in the matrix. Vacancies may be incorporated in the zones, as indicated by small squares.

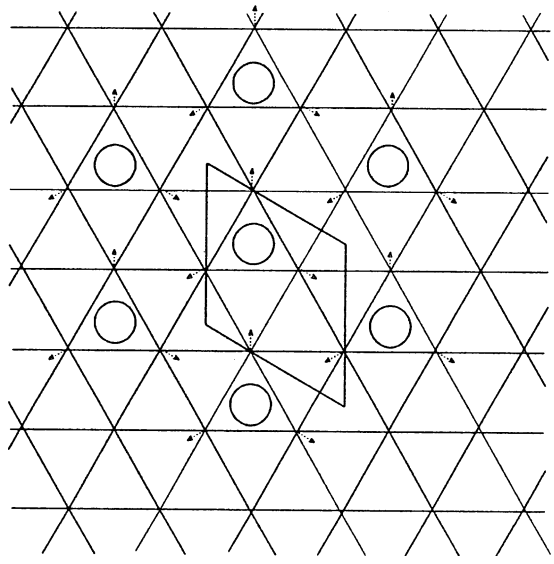

Fig. 12. Model of the relation between aluminum matrix and η', after Li *et al.* [8]. The hexagonal net of lines represents aluminum matrix positions in one {111} plane. Large circles indicate Mg atoms in the layer above this plan, at positions corresponding to the η'-structure. Resulting shifts of Zn-atoms relative to "ideal" positions of Al matrix are indicated by arrows, to produce one Zn-layer of η'.

from their original, matrix positions are associated with the Mg-atoms in the neighboring layer, see [8] for further details. GP(II) is assumed to be a precursor to η', and it seems likely that a similar mechanism occurs here, in a less ordered fashion. Some aspects of tentative models are sketched in Fig. 11. Figure 11(b) serves to suggest that Zn-rows in three <110> directions may occur in one {111} GP(II)-zone. In Fig. 11(c) the displacement of Zn-atoms from the ideal matrix lattice positions in the sheet is compensated by atom displacements associated with Mg-atoms in the layer above (or below). Note that when the proposed ordering of the Mg-atoms and associated Zn-displacements are completed, the η' precipitate becomes hexagonal, and coherent with the matrix. The formation of GP(II) may be linked with quenched-in vacancies from the solution treatment, presumably in the form of VRC, or vacancy-related clusters; this is tentatively included in Fig. 11(c) by some vacant positions.

Thicker GP(II) zones were occasionally observed in the [011] projection, consisting of 4–6 atom layers, Fig. 8(c). These zones may represent transition stages between GP(II) and η'. Together with the fact that GP(II) is formed only after quenching from a sufficiently high solution temperature. This is seen as supporting the sequence (2) as a major transformation route; however, with the GP(II) inserted as an intermediate stage:

$$\text{solid solution}(\alpha) \rightarrow \text{VRC} \rightarrow \text{GP(II)} \rightarrow \eta' \rightarrow \eta\text{-MgZn}_2 \tag{3}$$

The origin of the diffuse arcs shown in Fig. 5 is not clear, but their general shape suggests that they are associated with atomic displacements. The radius of the arcs corresponds to 0.233 nm, i.e. to $d_{111,Al}$, with some angular variation. From the appearance in different projections, we can reconstruct an extended curved streak in the {110} reciprocal plane. The diffuse arcs are most prominent in the very early stage of the aging at 100°C—before a strong GP(II)-pattern has developed. The diffuse arcs were not observed after RT-aging, it is therefore suggested as an early stage of GP(II)-formation, possibly originating from the "vacancy-related clusters".

The combination of these studies and the HRTEM-work on the structure of η' reported earlier [8] offers a structural description of the formation of the main hardening precipitate, with equation (3) as the most important precipitation sequence during two-stage aging. The vacancy-related cluster has not been observed, see however Curratis *et al*. [36] who noted that Frank loops are formed after quenching from temperatures above 490°C in an Al–Zn–Mg alloy. The diffuse streaks or arcs seen after very short aging time at 100°C may indicate that an early association of the clusters at this temperature may initiate the formation of GP(II)-zones. The distribution of GP(II)-zones is difficult to evaluate by TEM-method, the diffraction contrast is poorly defined, as seen from the dark-field image in Fig. 7. Diffraction observations indicate appreciable variations in the content of GP(II)-zones in the material, even between grains in the same sample. This may be due to variations in the vacancy or VRC-content at the start of GP(II)-zone formation, resulting from local vacancy sinks. It should be mentioned that the hardening precipitate η' can be formed also in situations where GP(II) was not found, viz. after quenching from lower solution temperatures. Hence several precipitation sequences may operate. The structural features of the GP(II) zones revealed by the diffraction patterns can be discussed in relation to the precipitation sequence (3) for η' and η: the formation of zinc-rich {111} layers may depend on associated magnesium atoms that can relieve local strain. When the magnesium atoms are ordered, and several GP(II)-zones associate to form a thicker zone, the zinc-atoms move into positions corresponding to the Zn/Al-plane in η', often with considerable disorder within the η'-precipitate [8]. In that paper a model for further atomic displacements during transformation to the equilibrium phase η-$MgZn_2$ was suggested. At the lower end of the sequence (3) there is still little direct evidence on the nature of the vacancy-related cluster. A detailed discussion was given by Katz and Ryum [18]: the VRC are formed by quenching from a temperature that is sufficiently high to produce a vacancy super-saturation above a critical value, depending upon alloy composition. For the clusters to develop into GP(II)-zones it appears that the temperature has to be raised to about 100°C, which then may be associated with the mobility of magnesium.

5. CONCLUSION

The two types of GP-zones in the Al–Zn–Mg alloy system are characterized by their electron diffraction patterns. GP(I)-zones are formed over a wide temperature range, from room temperature to 140–150°C, independently of quenching temperature. The zones are coherent with the aluminum matrix, with internal ordering of Zn and Al or Mg on the matrix lattice, based on a AuCu(I)-type sub-unit, and periodic antiphase boundaries. GP(II) are formed after quenching from temperatures above 450°C, by aging at temperatures above 70°C. Based on diffraction evidence the GP(II)-zones are described as zinc-rich layers on {111}-planes, with internal order in the form of elongated <110> domains. HRTEM-images along <110> and <111> direction are consistent with this interpretation. Structural relation of GP(II) to the previously published model for the η'-precipitate is discussed.

Acknowledgements—Financial support from the Norwegian Research Council is gratefully acknowledged.

REFERENCES

1. Guinier, A., *Compte Rend.*, 1938, **206**, 164.
2. Preston, G. D., *Proc Roy Soc. A*, 1938, **167**, 526.
3. Friauf, J. B., *Phys. Rev.*, 1927, **29**, 35.
4. Komura, Y. and Tokunaga, K., *Acta cryst.*, 1980, **B36**, 1548.
5. Gjønnes, J. and Simensen, C., *Acta metall.*, 1970, **18**, 881.
6. Degischer, H. D., Lacom, W., Zahra, A. M. and Zahra, C. Y., *Z. Metallk.*, 1980, **71**, 231.
7. Auld, H. and Cousland, S. M., *Austr. J. Metal.*, 1974, **19**, 194.
8. Li, X. Z., Hansen, V., Gjønnes, J. and Wallenberg, L. R., *Acta mater.*, 1999, **47**, 2651.
9. Ringer, S. P. and Hono, K., *Mater. Char.*, 2000, **44**, 101.
10. Schmalzried, H. and Gerold, V., *Z. Metallk.*, 1958, **49**, 291.
11. Graf, R., *C.R. Acad. Sci.*, 1957, **244**, 337.
12. Lorimer, G. W. and Nicholson, R. B., *Acta metall.*, 1966, **14**, 1009.
13. Pashley, D. W., Jacobs, M. H. and Vietz, J. T., *Phil. Mag.*, 1967, **16**, 51.
14. Lyman, C. E. and Vandersande, J. B., *Metal. Trans. A*, 1976, **74**, 1211.
15. Panseri, C. and Federighi, T., *Phil. Mag.*, 1958, **3**, 1223.
16. Embury, J. D. and Nicholson, R. B., *Acta metall.*, 1965, **13**, 403.
17. Ryum, N., *Z. Metallkd.*, 1975, **66**, 338, 344.
18. Katz, Z. and Ryum, N., *Scripta metall.*, 1980, **15**, 265.
19. Löffler, H., Schulze, D., Wendick, G. and Kroggel, R., *Cryst. Res. Tech.*, 1983, **22**, 615.
20. Lendvai, J., *Mater. Sci. Forum*, 1996, **217–222**, 43.
21. Lacom, W., Degischer, H. P., Zahra, A. M. and Zahra, C. Y., *Scripta metall.*, 1980, **14**, 253.
22. Jiang, X. J., Noble, B., Hansen, V. and Taftø, J., *Metall. Mater. Trans. A*, 2001, **32A**, 1063.
23. Dlubek, G. and Gerber, W., *Phys Stat sol b*, 1991, **163**, 83.
24. Ferragut, R., Somoza, A. and Tolley, A., *Acta mater.*, 1999, **47**, 4355.
25. Lendvai, J., Kovacs, I., Ungar, T., Lakner, J. and Baizs, K., *Aluminium*, 1980, **56**, 453.

26. Dünkeloh, K. H., Kralik, G. and Gerold, V., *Z. Metallkd.*, 1974, **65**, 291.
27. Park, J. K. and Ardell, A. J., *Metal. Trans. A*, 1957, **1983**, 14.
28. Thomas, G. and Nutting, J., *J. Inst. Metals*, 1959–60, **88**, 81.
29. Brofman, P. J. and Judd, G., *Metal. Trans.*, 1978, **94**, 457.
30. Ortner, S. R., Grovenor, C. R. M. and Shollock, B. A., *Scripta metall.*, 1988, **22**, 839.
31. Zhou, Z. K., Du, K. and Li, D. X., *Proc. ICEM 14, Cancun. Mexico, 31 August–4 September*, 1998, Vol. II, p. 11.
32. Mukhopadhyay, A. K., *Phil. Mag. Lett.*, 1994, **70**, 135.
33. Hono, K., Sano, N. and Sakurai, T., *Surf. Sci.*, 1992, **266**, 350.
34. Stiller, K. K., Warren, P. J., Hansen, V., Angenete, J. and Gjønnes, J., *Mater. Sci. Eng. A*, 1999, **270**, 55.
35. Waterloo, G., Hansen, V., Gjønnes, J. and Skjervold, S. R., *Mater. Sci.Eng. A*, 2001, **303**, 226.
36. Curratis, P., Kroggel, R. and Wolter, R., *Z. Metallkd.*, 1987, **78**, 268.